




Molecular-excited-state calculations with the qubit-excitation-based adaptive variational quantum eigensolver protocol

Yordan S. Yordanov ^{1,2}, Crispin H. W. Barnes,¹ and David R. M. Arvidsson-Shukur ^{2,1}

¹*Cavendish Laboratory, Department of Physics, University of Cambridge, Cambridge CB3 0HE, United Kingdom*

²*Hitachi Cambridge Laboratory, J. J. Thomson Avenue, Cambridge CB3 0HE, United Kingdom*

 (Received 1 November 2021; revised 7 January 2022; accepted 9 September 2022; published 29 September 2022)

Calculations of molecular spectral properties, like photodissociation rates and absorption bands, rely on knowledge of the excited state energies of the molecule of interest. Protocols based on the variational quantum eigensolver (VQE) are promising candidates to calculate such energies on emerging noisy intermediate-scale quantum (NISQ) computers. The successful implementation of these protocols on NISQ computers, relies on ansätze that can accurately approximate the molecular states and that can be implemented by shallow quantum circuits. We introduce the excited qubit-excitation-based adaptive (e-QEB-ADAPT)-VQE protocol to calculate molecular-excited-state energies. The e-QEB-ADAPT-VQE constructs efficient problem-tailored ansätze by iteratively appending evolutions of qubit excitation operators. The e-QEB-ADAPT-VQE also improves on previous ADAPT-VQE protocol in that it is designed to be independent on the choice of initial reference state. We perform classical numerical simulations for LiH and BeH₂ to benchmark the performance of the e-QEB-ADAPT-VQE. We demonstrate that the e-QEB-ADAPT-VQE can construct highly accurate ansätze that require at least an order of magnitude fewer CNOT gates than standard fixed unitary coupled-cluster ansätze, such as the UCCSD and the GUCCSD. We also show that the e-QEB-ADAPT-VQE is more successful in constructing ansätze for excited molecular states than other ADAPT-VQE protocols.

DOI: [10.1103/PhysRevA.106.032434](https://doi.org/10.1103/PhysRevA.106.032434)

I. INTRODUCTION

Quantum molecular simulations with the variational quantum eigensolver (VQE) [1–6] are a promising application for emerging noisy intermediate-scale quantum (NISQ) [7–10] computers. The VQE is a hybrid quantum-classical algorithm that utilizes the Rayleigh-Ritz variational principle to determine the lowest eigenvalue of a Hamiltonian operator, H , by optimizing an ansatz. In particular the VQE can be used to solve the electronic structure problem [11] and find the ground-state configuration and energy of a molecule. By utilizing both a quantum and a classical computer, the VQE is less quantum hardware demanding at the expense of requiring more quantum measurements and classical postprocessing, as compared to purely quantum algorithms, like the quantum phase estimation (QPE) algorithm [12–14]. A major challenge for the practical realization of a molecular VQE simulation on NISQ computers is to construct a variationally flexible ansatz that (i) accurately approximates the ground eigenstate of H , (ii) is easy to optimize, and (iii) can be implemented by a shallow circuit that uses few two-qubit entangling gates, e.g., CNOT gates, which are the current bottleneck of NISQ computers [8].

The most widely used type of ansätze for molecular VQE simulations are the unitary coupled-cluster (UCC) ansätze [1,15–20]. They were motivated by the classical coupled-cluster theory [11] and correspond to products of fermionic excitation evolutions. Due to their fermionic structure, UCC ansätze preserve many of the physical symmetries of

electronic wave functions, which makes them accurate and easy to optimize at the same time. State of the art ADAPT-VQE protocols [20–24] iteratively construct problem-tailored ansätze, which consist of close to optimal numbers of fermionic excitation evolutions. These ansätze are implemented by shallow ansatz circuits and have few variational parameters, while at the same time they are highly accurate.

In a previous work [25], we introduced the qubit-excitation-based adaptive (QEB-ADAPT)-VQE. Unlike the original fermionic-ADAPT-VQE [21], the QEB-ADAPT-VQE constructs a problem-tailored ansatz by appending “qubit excitation evolutions” (unitary evolutions of excitation operators that satisfy “qubit commutation relations” [25–28]). Qubit excitation evolutions are implemented by circuits simpler than those of the standard fermionic excitation evolutions [27]. Also, as demonstrated in Refs. [22,25,28], both types of excitation evolutions approximate electronic wave functions comparably well. Thus, in Ref. [25] we demonstrated that the QEB-ADAPT-VQE can simulate molecular ground states, using quantum circuits that are shallower than those of the previous state of the art fermionic-ADAPT-VQE [21] and qubit-ADAPT-VQE [22] protocols.

The VQE can also be used to solve the more general problem of finding excited-state energies [29–34]. In this work, we present a modified version of the QEB-ADAPT-VQE designed to simulate molecular excited states, which we call the excited (e)-QEB-ADAPT-VQE. The QEB-ADAPT-VQE, similarly to other VQE protocols, largely relies on an initial reference state, $|\psi_0\rangle$, that has a large overlap with the

true ground state, $|E_0\rangle$. In particular, the QEB-ADAPT-VQE evaluates the energy gradients of individual qubit excitation evolutions in order to decide the best way to grow its ansatz at each iteration. These energy gradients are evaluated for zero values of the variational parameters on the presumption that $|\psi_0\rangle$ is close to $|E_0\rangle$. However, choosing an initial reference state that has a significant overlap with an unknown excited state is challenging. We modify the ansatz-growing strategy of the QEB-ADAPT-VQE, so that it does not require $|\psi_0\rangle$ to be close to the target (ground or excited) state. Additionally, we present a comparison of qubit and fermionic excitation evolutions in their ability to construct ansätze for excited states.

The paper is organized as follows. In Sec. II we give a theoretical introduction. Section III describes the steps of the e-QEB-ADAPT-VQE protocol, and in Sec. IV we benchmark its performance for the first excited states of LiH and BeH₂. Lastly, Sec. V presents a comparison between qubit and fermionic excitation evolutions.

II. THEORY

A. The electronic structure problem and the variational quantum eigensolver

Finding the ground state $|E_0\rangle$ and the corresponding energy E_0 of a molecule is known as the “electronic structure problem” [11]. This problem can be solved by solving the time-independent Schrödinger equation $H|E_0\rangle = E_0|E_0\rangle$, where H is the electronic Hamiltonian of the molecule. Within the Born-Oppenheimer approximation, where the nuclei of the molecule are assumed to be motionless, H can be written in second quantized form as

$$H = \sum_{i,k}^{N_{\text{MO}}} h_{i,k} a_i^\dagger a_k + \sum_{i,j,k,l}^{N_{\text{MO}}} h_{i,j,k,l} a_i^\dagger a_j^\dagger a_k a_l. \quad (1)$$

Here, N_{MO} is the number of considered spin-orbitals, a_i^\dagger and a_i are the fermionic ladder operators, corresponding to the i th molecular spin-orbital, and the factors h_{ij} and h_{ijkl} are one- and two-electron integrals, written in a spin-orbital basis [11]. The Hamiltonian expression in Eq. (1) can be mapped to quantum-gate operators using a qubit-encoding method, e.g., the Jordan-Wigner (JW) [35] or the Bravyi-Kitaev [36,37] methods. Throughout this work, we assume the more straightforward JW encoding, where the occupancy of the i th molecular spin-orbital is represented by the state of the i th qubit.

The fermionic ladder operators a_i^\dagger and a_i satisfy anticommutation relations

$$\{a_i, a_j^\dagger\} = \delta_{i,j}, \quad \{a_i, a_j\} = \{a_i^\dagger, a_j^\dagger\} = 0. \quad (2)$$

Within the JW encoding, a_i^\dagger and a_i can be written in terms of quantum gate operators as

$$a_i^\dagger = Q_i^\dagger \prod_{r=0}^{i-1} Z_r = \frac{1}{2}(X_i - iY_i) \prod_{r=0}^{i-1} Z_r \quad \text{and} \quad (3)$$

$$a_i = Q_i \prod_{r=0}^{i-1} Z_r = \frac{1}{2}(X_i + iY_i) \prod_{r=0}^{i-1} Z_r, \quad (4)$$

where

$$Q_i^\dagger \equiv \frac{1}{2}(X_i - iY_i) \quad \text{and} \quad Q_i \equiv \frac{1}{2}(X_i + iY_i). \quad (5)$$

We refer to Q_i^\dagger and Q_i as qubit creation and annihilation operators, respectively. The operators Q_i^\dagger and Q_i satisfy the “qubit commutation relations” [25–27]

$$\{Q_i, Q_j^\dagger\} = I, \quad [Q_i, Q_j^\dagger] = 0 \quad \text{if } i \neq j, \quad \text{and} \\ [Q_i, Q_j] = [Q_j^\dagger, Q_i^\dagger] = 0 \quad \text{for all } i, j. \quad (6)$$

We use Q_i^\dagger and Q_i in Sec. II B to define qubit excitation evolutions.

Substituting Eqs. (3) and (4) into Eq. (1), H can be written as

$$H = \sum_{r=0}^{N_H-1} h_r \prod_{s=0}^{N_{\text{MO}}-1} \sigma_s^t, \quad (7)$$

where σ_s^t is a Pauli operator (X_s , Y_s , Z_s , or I_s) acting on qubit s , h_r (not to be confused with h_{ik} and h_{ijkl}) is a real scalar coefficient, and N_H is the number of Pauli terms in the representation of H . N_H scales as $O(N_{\text{MO}}^4)$. The expectation value of H can be evaluated by individually measuring on a quantum computer the expectation values of all Pauli string terms in Eq. (7).

Once H is mapped to a Pauli string representation, the VQE can be used to minimize the expectation value $E(\theta) = \langle \psi(\theta) | H | \psi(\theta) \rangle$, where $|\psi(\theta)\rangle$ is a trial state. The VQE relies upon the Rayleigh-Ritz variational principle [38]

$$\langle \psi(\theta) | H | \psi(\theta) \rangle \geq E_0 \quad (8)$$

to find an upper-bounded estimate for E_0 . The VQE is a hybrid-quantum-classical algorithm that uses a quantum computer to prepare the trial state $|\psi(\theta)\rangle$ and evaluate $E(\theta)$ and a classical computer to process the measurement data and update θ at each iteration. The trial state $|\psi(\theta)\rangle = U(\theta)|\psi_0\rangle$ is generated by the ansatz $U(\theta)$ applied to an initial reference state $|\psi_0\rangle$.

B. Qubit and fermionic excitation evolutions

The most widely used type of ansätze for molecular VQE simulations are the unitary coupled-cluster (UCC) ansätze, motivated by the classical coupled-cluster method [11]. UCC ansätze are constructed as products of fermionic excitation evolutions. The QEB-ADAPT-VQE and the e-QEB-ADAPT-VQE instead construct ansätze that consist of qubit excitation evolutions. This subsection provides definitions of the two types of unitary operations.

1. Fermionic excitation evolutions

Single and double fermionic excitation operators are defined, respectively, by the skew-Hermitian operators

$$T_{ik} \equiv a_i^\dagger a_k - a_k^\dagger a_i \quad \text{and} \quad (9)$$

$$T_{ijkl} \equiv a_i^\dagger a_j^\dagger a_k a_l - a_k^\dagger a_l^\dagger a_i a_j. \quad (10)$$

Single and double fermionic excitation evolutions are thus given, respectively, by the unitary operators

$$A_{ik}(\theta) = e^{\theta T_{ik}} = \exp[\theta(a_i^\dagger a_k - a_k^\dagger a_i)] \quad \text{and} \quad (11)$$

$$A_{ijkl}(\theta) = e^{\theta T_{ijkl}} = \exp[\theta(a_i^\dagger a_j^\dagger a_k a_l - a_k^\dagger a_l^\dagger a_i a_j)]. \quad (12)$$

Using Eqs. (3) and (4), for $i < j < k < l$, A_{ik} and A_{ijkl} can be expressed in terms of quantum gate operators as

$$A_{ij}(\theta) = \exp\left[i\frac{\theta}{2}(X_i Y_j - Y_i X_j) \prod_{r=i+1}^{j-1} Z_r\right] \quad \text{and} \quad (13)$$

$$A_{ijkl}(\theta) = \exp\left[i\frac{\theta}{8}(X_i Y_j X_k X_l + Y_i X_j X_k X_l + Y_i Y_j Y_k X_l + Y_i Y_j X_k Y_l - X_i X_j Y_k X_l - X_i X_j X_k Y_l - Y_i X_j Y_k Y_l - X_i Y_j Y_k Y_l) \prod_{r=i+1}^{j-1} Z_r \prod_{r'=k+1}^{l-1} Z_{r'}\right]. \quad (14)$$

CNOT-efficient circuits to implemented single and double fermionic excitation evolutions were derived in Ref. [27].

2. Qubit excitation evolutions

Qubit excitation evolutions are generated by ‘‘qubit excitation operators.’’ Single and double qubit excitation operators are defined, respectively, by the skew-Hermitian operators

$$\tilde{T}_{ik} = Q_i^\dagger Q_k - Q_k^\dagger Q_i \quad \text{and} \quad (15)$$

$$\tilde{T}_{ijkl} = Q_i^\dagger Q_j^\dagger Q_k Q_l - Q_k^\dagger Q_l^\dagger Q_i Q_j. \quad (16)$$

Hence, single and double qubit excitation evolutions are defined, respectively, by the unitary operators

$$\tilde{A}_{ik}(\theta) = e^{\theta \tilde{T}_{ik}} = \exp[\theta(Q_i^\dagger Q_k - Q_k^\dagger Q_i)] \quad \text{and} \quad (17)$$

$$\tilde{A}_{ijkl}(\theta) = e^{\theta \tilde{T}_{ijkl}} = \exp[\theta(Q_i^\dagger Q_j^\dagger Q_k Q_l - Q_k^\dagger Q_l^\dagger Q_i Q_j)]. \quad (18)$$

Using Eq. (5), \tilde{A}_{ik} and \tilde{A}_{ijkl} can be re-expressed in terms of quantum gate operators:

$$\tilde{A}_{ik}(\theta) = \exp\left[i\frac{\theta}{2}(X_i Y_k - Y_i X_k)\right] \quad \text{and} \quad (19)$$

$$\tilde{A}_{ijkl}(\theta) = \exp\left[i\frac{\theta}{8}(X_i Y_j X_k X_l + Y_i X_j X_k X_l + Y_i Y_j Y_k X_l + Y_i Y_j X_k Y_l - X_i X_j Y_k X_l - X_i X_j X_k Y_l - Y_i X_j Y_k Y_l - X_i Y_j Y_k Y_l)\right]. \quad (20)$$

CNOT-efficient circuits to implement single and double qubit excitation evolutions were derived in Ref. [27].

C. Finding excited-state energies with the VQE

The two most common methods to calculate excited-state energies with the VQE are the quantum subspace expansion [39–41], and the overlap-based method [42,43]. In this work we use the latter, the overlap-based method.

As the name suggests the overlap-based method works by including the overlap between previously found eigenstates

of H and the state we are currently searching for in the cost function of the VQE. For example, after we find the ground state $|E_0\rangle$ we modify H as

$$H \rightarrow H_1 = H + \alpha_0 |E_0\rangle\langle E_0|, \quad (21)$$

where α_0 is a real positive scalar coefficient. If $\alpha_0 + E_0 > E_1$,¹ where E_1 is the energy of the first excited state of H , the lowest energy eigenvalue of the modified Hamiltonian H_1 will be shifted to E_1 . Hence, running the VQE for H_1 should output an estimate for E_1 :

$$E_1 = \min_{\theta_1} \langle \psi_0 | U_1^\dagger(\theta_1) H_1 U_1(\theta_1) | \psi_0 \rangle \\ = \min_{\theta_1} \langle \psi_0 | U_1^\dagger(\theta_1) (H + \alpha_0 |E_0\rangle\langle E_0|) U_1(\theta_1) | \psi_0 \rangle. \quad (22)$$

After E_1 is found the same procedure can be repeated recursively multiple times to find the next energy eigenvalues of H . The k th energy eigenvalue of H , E_k , can be estimated as

$$E_1 = \min_{\theta_k} \langle \psi_0 | U_k^\dagger(\theta_k) H_k U_k(\theta_k) | \psi_0 \rangle \\ = \min_{\theta_k} \langle \psi_0 | U_k^\dagger(\theta_k) (H + \sum_{r=0}^{k-1} \alpha_r |E_r\rangle\langle E_r|) U_k(\theta_k) | \psi_0 \rangle. \quad (23)$$

The first term in Eq. (23), is calculated as described above, by measuring the expectation values of the Pauli string terms in the expression for H [Eq. (7)]. The overlap terms in Eq. (23) can be calculated with the SWAP test [44].

III. THE e-QEB-ADAPT-VQE

The e-QEB-ADAPT-VQE algorithm finds an estimate for the k th excited state of an electronic Hamiltonian, H , by constructing a problem-tailored ansatz. The ansatz is constructed by iteratively appending qubit excitation evolutions, based on the greedy strategy to obtain the lowest estimate for the energy, $E(\theta)$, at each iteration. In this subsection, we describe the preparation components, and the iterative ansatz-constructing loop, of the e-QEB-ADAPT-VQE algorithm. For a description of the original QEB-ADAPT-VQE, we refer the reader to Ref. [25].

First, we transform H to a quantum-gate-operator representation as described in Sec. II A. This involves the calculation of the one- and two-electron integrals, h_{ik} and h_{ijkl} [Eq. (1)], which can be done efficiently (in time polynomial in N_{MO}) on a classical computer. If we want to find the energy of the excited state $|E_k\rangle$, E_k , we add the additional overlap terms to H , as described in Sec. II C, to get H_k .

Second, we define an ansatz element pool $\mathbb{P}(\tilde{A}, N_{\text{MO}})$ of all unique single and double qubit excitations, $\tilde{A}_{ik}(\theta)$ and $\tilde{A}_{ijkl}(\theta)$, respectively, for $i, j, k, l \in \{0, N_{\text{MO}} - 1\}$. The size of this pool is $|\mathbb{P}(\tilde{A}, N_{\text{MO}})| = \binom{N_{\text{MO}}}{2} + 3\binom{N_{\text{MO}}}{4}$.

Third, we choose an initial reference state $|\psi_0\rangle$. As we mentioned in the Introduction, the performance of the e-QEB-ADAPT-VQE is intended to be independent of the choice of

¹To make sure that $\alpha_0 + E_0 > E_1$, prior to knowing E_1 , we can choose an arbitrary value for α_0 , which is large compared to the energy scale of the problem.

$|\psi_0\rangle$. Hence, we arbitrarily choose the initial reference state to be the Hartree-Fock state, but in principle any computational basis state with a Hamming weight equal to the number of electrons N_e will do.

Now we are ready to begin constructing the ansatz. We set the iteration number to $m = 1$, set the ansatz to the identity $U \rightarrow U^{(0)} = I$, and initiate the iterative ansatz-constructing loop. We describe the five steps of the m th iteration below. Afterwards we comment on these steps.

(i) Prepare trial state $|\psi^{[m-1]}\rangle = U(\theta^{[m-1]})|\psi_0\rangle$, with values for $\theta^{[m-1]}$ as determined in the previous iteration.

(ii) For each (single or double) qubit excitation evolution $\tilde{A}_p(\theta_p) \in \mathbb{P}(\tilde{A}, N_{\text{MO}})$,

(a) run the VQE to find

$$\min_{\theta_p} E(\theta_p) = \min_{\theta_p} \langle \psi^{[m-1]} | \tilde{A}_p^\dagger(\theta_p) H_k \tilde{A}_p(\theta_p) | \psi^{[m-1]} \rangle, \text{ and}$$

(b) calculate the energy reduction magnitude $E^{[m-1]} - \min_{\theta_p} E(\theta_p)$.

(iii) Identify the set of n qubit excitation evolutions, $\tilde{\mathbb{A}}^{[m]}(n)$, corresponding to the n largest energy reductions in the previous step. For $\tilde{A}_p(\theta_p) \in \tilde{\mathbb{A}}^{[m]}(n)$,

(a) run the VQE to find $\min_{\theta^{[m-1]}, \theta_p} E(\theta^{[m-1]}, \theta_p)$

$$= \min_{\theta^{[m-1]}, \theta_p} \langle \psi_0 | U^\dagger(\theta^{[m-1]}) \tilde{A}_p^\dagger(\theta_p) H_k \tilde{A}_p(\theta_p) U(\theta^{[m-1]}) | \psi_0 \rangle,$$

(b) calculate the energy reduction $\Delta E_p^{[m]} = E^{[m-1]} - \min_{\theta^{[m-1]}, \theta_p} E(\theta^{[m-1]}, \theta_p)$, and

(c) save the (re)optimized values of $\theta^{[m-1]} \cup \{\theta_p\}$ as $\theta_p^{[m]}$.

(iv) Identify the qubit excitation evolution $\tilde{A}^{[m]}(\theta^{[m]}) \equiv \tilde{A}_{p'}(\theta_{p'})$ corresponding to the largest energy reduction $\Delta E^{[m]} \equiv \Delta E_{p'}^{[m]}$ in the previous step.

If $\Delta E^{[m]} < \epsilon$, where $\epsilon > 0$ is an energy threshold,

(a) exit,

or else:

(a) append $\tilde{A}^{[m]}(\theta^{[m]})$ to the ansatz,

$$U(\theta^{[m-1]}) \rightarrow U(\theta^{[m]}) = \tilde{A}^{[m]}(\theta^{[m]})U(\theta^{[m-1]}), \quad (24)$$

(b) set $E^{[m]} = E^{[m-1]} - \Delta E_p^{[m]}$, and

(c) set the values of the new set of variational parameters, $\theta^{[m]} = \theta^{[m-1]} \cup \{\theta_{p'}\}$, to $\theta_{p'}^{[m]}$.

(v) Enter the $m + 1$ iteration by returning to step 1.

We now elaborate on the steps outlined above.

The m th iteration of the e-QEB-ADAPT-VQE starts by preparing the trial state $|\psi^{[m-1]}\rangle$ obtained in the $(m - 1)$ th iteration.

At each iteration we aim to identify the qubit excitation evolution that, when appended to the ansatz, would maximize the energy reduction $E(\theta^{[m-1]}) - E(\theta^{[m]})$. To identify such a qubit excitation evolution, first we calculate [step (ii)] the individual energy reduction contributions of each qubit excitation evolution $\tilde{A}_p(\theta_p) \in \mathbb{P}(\tilde{A}, N_{\text{MO}})$. Each of these energy reductions is calculated by a single-parameter VQE optimization performed to minimize the energy expectation value $\langle \psi^{[m-1]} | \tilde{A}_p^\dagger(\theta_p) H \tilde{A}_p(\theta_p) | \psi^{[m-1]} \rangle$. In this way, we get an indication of by how much the energy expectation value

will be reduced when each $\tilde{A}_p(\theta_p)$ is appended to the ansatz $U(\theta^{[m-1]})$ and the energy is minimized along the full set of parameters $\theta^{[m-1]} \cup \{\theta_p\}$, at a reduced cost of performing $O(N_{\text{MO}}^4)$ single-parameter VQE optimizations (instead of $O(N_{\text{MO}}^4)$ m -parameter VQE optimizations).

In the original QEB-ADAPT-VQE such an indication is obtained by measuring the energy gradients $\{\frac{\partial}{\partial \theta_p} \langle \psi^{[m-1]} | \tilde{A}_p^\dagger(\theta_p) H \tilde{A}_p(\theta_p) | \psi^{[m-1]} \rangle\}$. However, these energy gradients must be evaluated for some values of the respective parameters $\{\theta_p\}$. If we are approximating the ground state $|E_0\rangle$ and we have a high level of confidence that $|\psi_0\rangle$ has a large overlap with $|E_0\rangle$, then the gradients can be evaluated conveniently for $\{\theta_p = 0\}$. But if we are approximating the excited state $|E_k\rangle$, where we do not know how close $|\psi_0\rangle$ and $|E_k\rangle$ are, measuring the energy gradients for $\{\theta_p = 0\}$, or any other arbitrary values of $\{\theta_p\}$, can be a poor indicator, leading to an inefficient and slow construction of the ansatz, and a possibility of getting stuck in local energy minimum (see Sec. IV A). Instead the e-QEB-ADAPT-VQE measures the individual energy reduction contribution for each qubit excitation evolution, which can be obtained by a single-parameter VQE optimization, using a direct-search minimizer [45], e.g., the Nelder-Mead method [46], irrespectively of the overlap of $|\psi_0\rangle$ and $|E_k\rangle$.

Calculating a single energy-gradient requires measuring $2N_H$ (N_H is the number of Pauli strings in the representation of H , see Eq. [7]) expectation values.² On the other hand, running a single-parameter VQE requires measuring γN_H expectation values, where γ is the number of function evaluations required for a single parameter minimization. Hence, the additional cost of the technique pursued here, in comparison to using energy gradients as in the original QEB-ADAPT-VQE, is a factor of $\gamma/2$ more quantum computer measurements in step (ii).³ In addition, once the ansatz reaches some critical size, so that $|\psi^{[m-1]}\rangle$ can be assumed to have a significant overlap with $|E_k\rangle$, we can switch to the cheaper QEB-ADAPT-VQE.

The individual energy reductions calculated in step (ii) indicate how much each qubit excitation evolution can decrease $E^{[m-1]}$ when appended to $U(\theta^{[m-1]})$. However, the largest individual energy reduction does not necessarily correspond to the largest energy reduction when the ansatz is optimized over all variational parameters. In step (iii), we identify the set of n qubit excitation evolutions with the individual energy reductions: $\tilde{\mathbb{A}}^{[m]}(n)$. We assume that $\tilde{\mathbb{A}}^{[m]}(n)$ likely contains the qubit excitation evolution that reduces $E^{[m-1]}$ the most. For each of the n qubit excitation evolutions in $\tilde{\mathbb{A}}^{[m]}(n)$, we run the VQE, for all variational parameters, with the ansatz from the previous iteration to calculate how much it contributes to the energy reduction. If multiple quantum devices are available, step (iii) can be parallelized.

²This follows from the fact that, in order to calculate the energy gradient of a qubit excitation evolution, we need to measure the commutator of the evolution and the Hamiltonian: $\frac{\partial}{\partial \theta_p} \langle \psi^{[m-1]} | \tilde{A}_p^\dagger(\theta_p) H \tilde{A}_p(\theta_p) | \psi^{[m-1]} \rangle = \langle \psi^{[m-1]} | [H \tilde{A}_p(\theta_p)] | \psi^{[m-1]} \rangle$ [21,25].

³For the Nelder-Mead method, γ is on the order of 10.

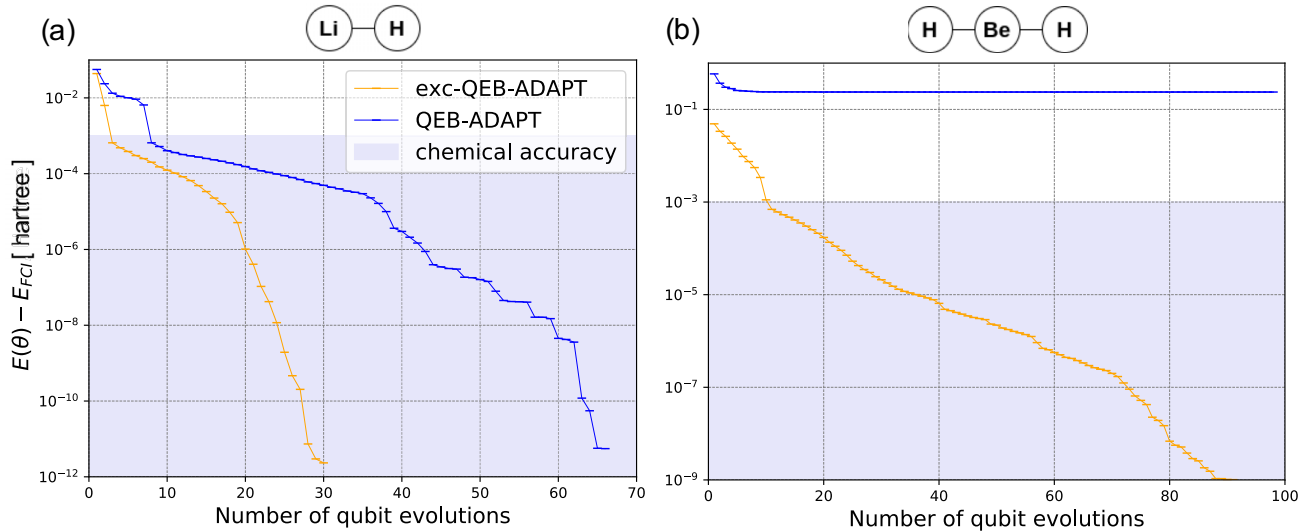


FIG. 1. Energy convergence plots for the first excited states of LiH and BeH₂ in the STO-3G basis at equilibrium bond distances of $r_{\text{Li-H}} = 1.546 \text{ \AA}$ and $r_{\text{Be-H}} = 1.316 \text{ \AA}$, respectively. The plots are obtained with the QEB-ADAPT-VQE and the e-QEB-ADAPT-VQE for $n = 10$

In step (iv), we pick the qubit excitation evolution, $\tilde{A}^{[m]}(\theta^{[m]})$, corresponding to the largest energy reduction, $\Delta E^{[m]}$. If $\Delta E^{[m]}$ is below some threshold $\epsilon > 0$, we exit the iterative loop. If instead $|\Delta E^{[m]}| > \epsilon$, we add $\tilde{A}^{[m]}(\theta^{[m]})$ to the ansatz and begin the next iteration.

IV. BENCHMARKING THE e-QEB-ADAPT-VQE

In this section, we benchmark the performance of the e-QEB-ADAPT-VQE by finding the excited-state energies of LiH and BeH₂, which have been simulated on real quantum computers [1,47]. The results presented here are based on classical numerical VQE simulations, performed with a custom in-house code.⁴ The Hamiltonians for LiH and BeH₂ are represented in the STO-3G orbital basis set [48], with no frozen orbitals assumed. Hence, the wave function of LiH is represented by a 12-qubit state, and that of BeH₂ is represented by a 14-qubit state. In step (ii) of the e-QEB-ADAPT-VQE, the VQE optimization is performed with the direct-search Nelder-Mead method [46], and in step (iii) it is performed with the gradient-descent BFGS method [49]. In Sec. IV B we also perform classical numerical VQE simulations with the UCCSD and generalized UCCSD (GUCCSD) ansätze (which are used for comparison). For these simulations we use the BFGS method.

A. The QEB-ADAPT-VQE vs the e-QEB-ADAPT-VQE

In this subsection we compare the convergence rates, to the first-excited-state energies of LiH and BeH₂, of the QEB-ADAPT-VQE and the e-QEB-ADAPT-VQE. With this comparison we demonstrate that the energy-gradient-based ansatz-growing strategy of the QEB-ADAPT-VQE is unsuitable for excited states.

⁴The code and the numerical data are available upon request from the authors.

Figure 1 presents energy convergence plots for the first excited states of LiH and BeH₂ in the STO-3G basis at equilibrium bond distances of $r_{\text{Li-H}} = 1.546 \text{ \AA}$ and $r_{\text{Be-H}} = 1.316 \text{ \AA}$, respectively. The plots are obtained with each of the two protocols.

In the case of LiH the QEB-ADAPT-VQE converges slower, requiring more than twice as many ansatz-constructing iterations than the e-QEB-ADAPT-VQE. Since each ansatz-constructing iteration corresponds to a qubit excitation evolution in the ansatz, the ansatz constructed by the QEB-ADAPT-VQE is roughly twice as large as the one constructed by the e-QEB-ADAPT-VQE. As suggested in Sec. III above, the underlying reason for this is the inability of the energy-gradient-based ansatz-growing strategy of the QEB-ADAPT-VQE to grow an efficient ansatz when the initial reference state $|\psi_0\rangle$ does not have a significant overlap with the target excited state $|E_k\rangle$. In the case of BeH₂, the QEB-ADAPT-VQE completely fails to converge to chemical accuracy, likely getting stuck in a local energy minimum.

Nevertheless, the e-QEB-ADAPT-VQE, being independent on the overlap of $|\psi_0\rangle$ and $|E_k\rangle$, converges successfully for both molecules.

B. Energy dissociation curves

In this section, we benchmark the performance of the e-QEB-ADAPT-VQE, for $\epsilon = 10^{-6}$ hartree and $\epsilon = 10^{-8}$ hartree, by obtaining energy dissociation plots for the first excited states of LiH and BeH₂. For a comparison, we also include energy dissociation plots obtained with the VQE using the single-Trotterized standard UCCSD [15,16] ansatz, which consists of single and double fermionic excitation evolutions above the Hartree-Fock state, and the larger GUCCSD ansatz [17], which consists of all unique single and double fermionic excitation evolutions.

The energy dissociation curves for the two molecules are given in Figs. 2(a) and 2(b). Figures 2(c) and 2(d) show the

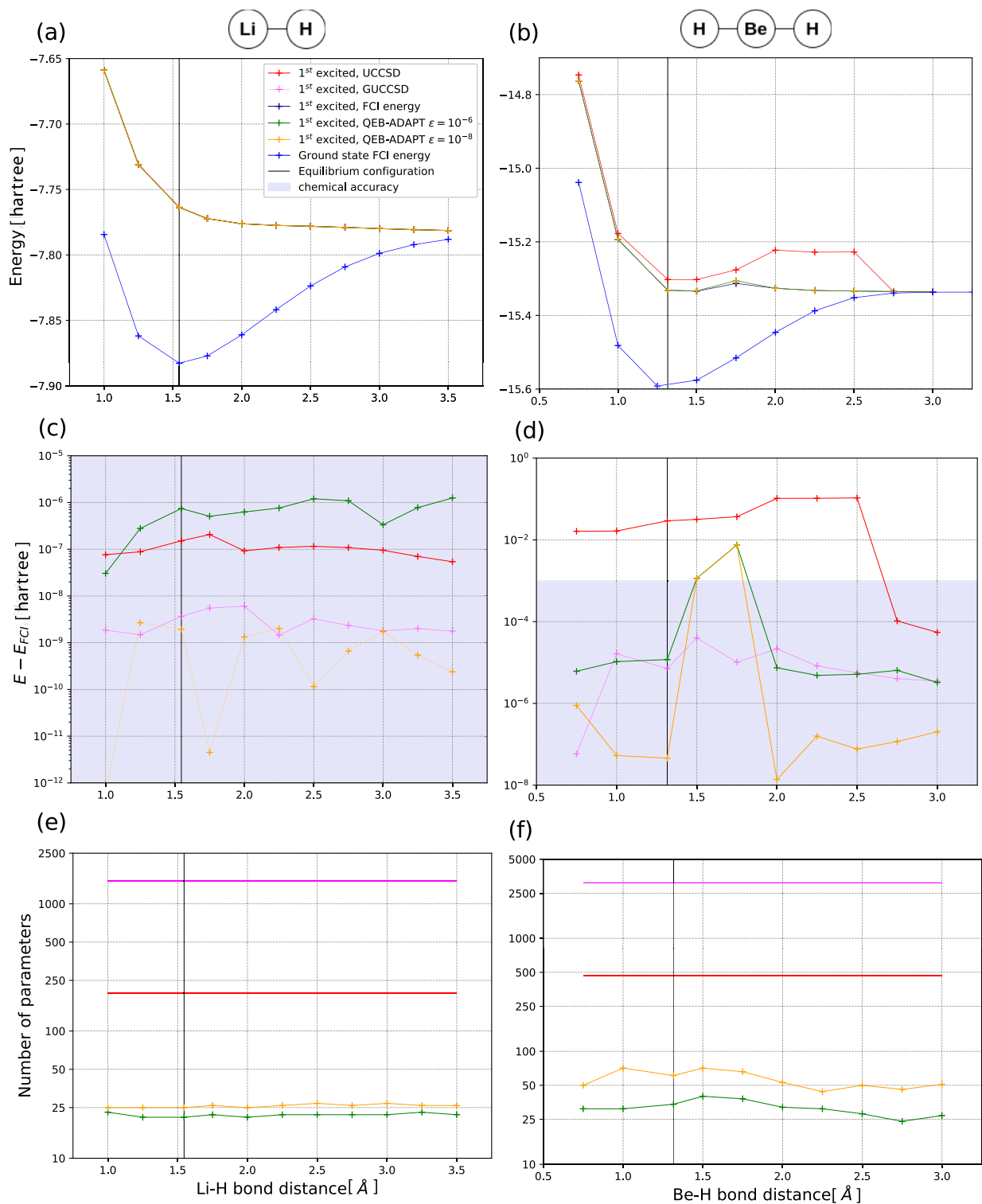


FIG. 2. Energy dissociation curves for LiH and BeH₂ in the STO-3G orbital basis. (a, b) Absolute values for the estimated first-excited-state energies. (c, d) Error in the estimated energy values with respect to the exact FCI energy. (e, f) Number of variational parameters, also equal to the number of qubit and fermionic evolutions, of the ansatz used by each method.

errors of each method with respect to the full configuration interaction (FCI) energy [11,50]. In the case of LiH, all methods achieve chemical accuracy. Figures 2(e) and 2(f) show the numbers of variational parameters, which are also equivalent

to the number of qubit and fermionic excitation evolutions, used in the ansatz of each method. The ansätze constructed by the e-QEB-ADAPT-VQE, for LiH, are extremely compact, consisting of at most 27 qubit evolutions, whereas the UCCSD

TABLE I. CNOT counts for the UCCSD ansatz, the GUCCSD ansatz, and the ansätze constructed by the e-QEB-ADAPT-VQE ($\epsilon = 10^{-8}$) for the first excited states of LiH and BeH₂ in the STO-3G basis.

	UCCSD	GUCCSD	e-QEB-ADAPT-VQE
LiH	3496	29 447	311
BeH ₂	8980	64 064	896

ansatz and the GUCCSD ansatz consist of 200 and 1521 fermionic evolutions, respectively.

In the case of BeH₂ the results are more complicated. First, the UCCSD-VQE fails to achieve chemical accuracy for the majority of bond distances [Fig. 2(d)]. This result is not surprising as the simple UCCSD ansatz is not suitable to approximate strongly correlated states such as excited states. Second, in Fig. 2(d) we see that the e-QEB-ADAPT-VQE fails to achieve chemical accuracy for bond distances of $r_{\text{Be-H}} = 1.5 \text{ \AA}$ and $r_{\text{Be-H}} = 1.75 \text{ \AA}$. We comment on the reason for this in Sec. IV C. The only method that achieves chemical accuracy at all bond distances is the GUCCSD-VQE, because of the highly variationally flexible GUCCSD ansatz. Nevertheless, for the majority of bond distances the e-QEB-ADAPT-VQE constructs ansätze that are more accurate and consist of nearly 50 times fewer ansatz elements than the GUCCSD ansatz [Figs. 2(d) and 2(f)].

These results together with the fact that qubit evolutions are implemented by circuits simpler than those of fermionic evolutions implies that the ansätze constructed by the e-QEB-ADAPT-VQE are implemented by much shallower circuits

that have much fewer CNOT gates than the UCCSD and GUCCSD ansätze. Table I summarizes the CNOT counts for the UCCSD and GUCCSD ansätze and for the ansätze constructed by the e-QEB-ADAPT-VQE ($\epsilon = 10^{-8}$) for each molecule. For the e-QEB-ADAPT-VQE ($\epsilon = 10^{-8}$), the maximum CNOT counts over all bond distances for each molecule are shown. As we can see in Table I, the ansätze constructed by the e-QEB-ADAPT-VQE use at least 10 times fewer CNOT gates than the UCCSD ansatz, and more than 60 times fewer CNOT gates than the GUCCSD ansatz.

C. Finding the wrong excited-state energy

As we saw in Fig. 2(d), the e-QEB-ADAPT-VQE fails to achieve chemical accuracy for BeH₂ at bond distances $r_{\text{Be-H}} = 1.5 \text{ \AA}$ and $r_{\text{Be-H}} = 1.75 \text{ \AA}$. In order to investigate the reason for this see Fig. 3, which depicts the FCI energies for the ten lowest energy states of BeH₂ (in the STO-3G basis) as a function of bond distance.

The nine excited states shown in Fig. 3 are ordered in three degenerate energy levels. Table II below summarizes the energy levels and their corresponding excited states at bond distances $r_{\text{Be-H}} = 1.5 \text{ \AA}$ and $r_{\text{Be-H}} = 1.75 \text{ \AA}$. For $r_{\text{Be-H}} = 1.5 \text{ \AA}$ we can see that $E_{\text{I}}(1.5 \text{ \AA})$ and $E_{\text{II}}(1.5 \text{ \AA})$ are very close. Upon inspection of the energy estimate of the e-QEB-ADAPT-VQE ($\epsilon = 10^{-8}$), for $r_{\text{Be-H}} = 1.5 \text{ \AA}$, it turns out that the algorithm actually finds $E_{\text{II}}(1.5 \text{ \AA})$ with an accuracy of 3×10^{-8} hartree. Therefore, the problem is not a lack of accuracy, but converging to the wrong excited state.

Two possible reasons for this are as follows: (i) the classical minimizers employed by the e-QEB-ADAPT-VQE get stuck

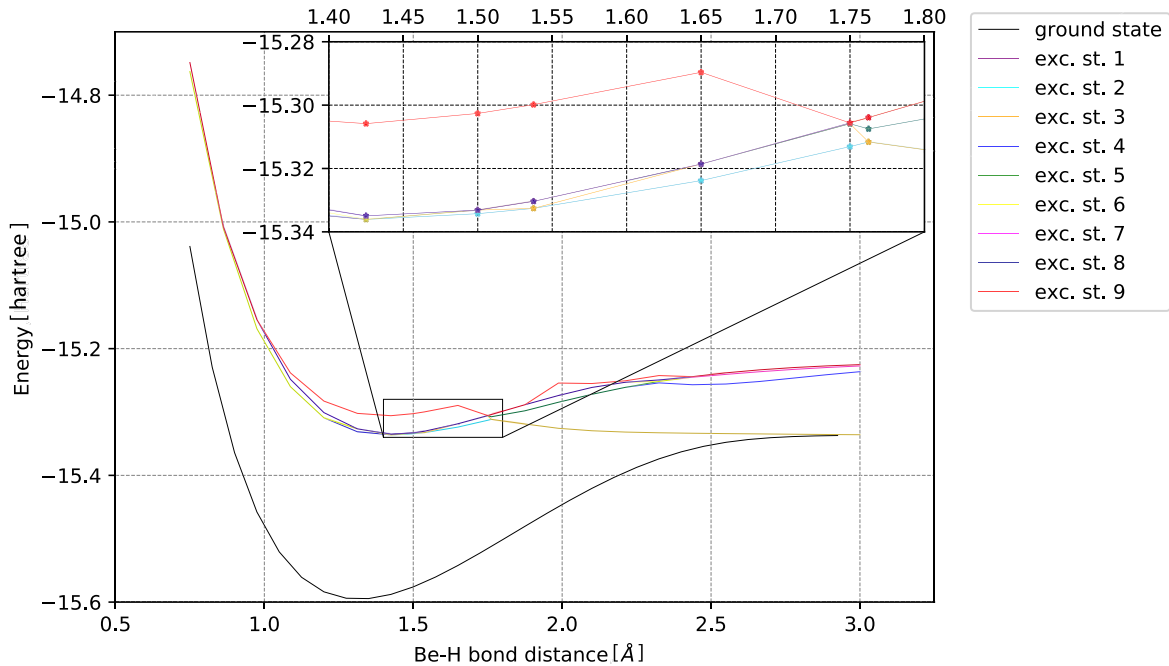


FIG. 3. FCI energies for the ten lowest energy states of BeH₂ in the STO-3G basis. The numbers of the excited states correspond to their order at the ground-state equilibrium bond distance of $r_{\text{Be-H}} = 1.316 \text{ \AA}$. Note that the discontinuities in the potential energy curve of excited state 9 are due to crossings with higher excited states that are not plotted.

TABLE II. Energy levels for the nine lowest excited states of BeH_2 in the STO-3G basis. The ground state (not shown) is counted as the 0th.

$r_{\text{Be-H}} = 1.5 \text{ \AA}$	
Exc. states	Energy (hartree)
{1,2}	$E_I(1.5 \text{ \AA}) \approx -15.3343$
{3,4,5,6,7,8}	$E_{II}(1.5 \text{ \AA}) \approx -15.3331$
{9}	$E_{III}(1.5 \text{ \AA}) \approx -15.3026$
$r_{\text{Be-H}} = 1.75 \text{ \AA}$	
Exc. states	Energy (hartree)
{1,2}	$E_I(1.75 \text{ \AA}) \approx -15.3131$
{3,4,5}	$E_{II}(1.75 \text{ \AA}) \approx -15.3059$
{6,7,8,9}	$E_{III}(1.75 \text{ \AA}) \approx -15.3056$

in a local minimum corresponding to $E_{II}(1.5 \text{ \AA})$, and/or (ii) the e-QEB-ADAPT-VQE fails to construct an ansatz that can approximate the degenerate excited states corresponding to the energy level $E_I(1.5 \text{ \AA})$. Since the e-QEB-ADAPT-VQE uses a combination of the BFGS and the Nelder-Mead optimization methods, where the Nelder-Mead is a direct-search method, which is unlikely to get stuck in local minimum, the first possible reason can be ruled out. Hence, we are left with the second one.

Upon explicit inspection of the degenerate states corresponding to the energy level $E_I(1.5 \text{ \AA})$, it is found that they have strong static correlations [50], where two dominant Slater determinants contribute equally to the wave function. On the other hand for each of the degenerate states corresponding to the energy level $E_{II}(1.5 \text{ \AA})$ there is one dominant Slater determinant. Hence, the first few ansatz-constructing iterations of the e-QEB-ADAPT-VQE grow the ansatz with qubit excitation evolutions, which map between the initial reference state $|\psi_0\rangle$ and the dominant Slater determinant of one of the states corresponding to $E_{II}(1.5 \text{ \AA})$, because these qubit excitation evolutions decrease the estimate for the energy by the most. From that point on, the e-QEB-ADAPT-VQE continues to construct an ansatz that approximates a state corresponding to $E_{II}(1.5 \text{ \AA})$, instead a state corresponding to $E_I(1.5 \text{ \AA})$.

In the case of $r_{\text{Be-H}} = 1.75 \text{ \AA}$, the situation is similar. However, in this case the three energy levels $E_I(1.75 \text{ \AA})$, $E_{II}(1.75 \text{ \AA})$, and $E_{III}(1.75 \text{ \AA})$ are close, and the QEB-ADAPT-VQE converges to an excited state corresponding to $E_{III}(1.75 \text{ \AA})$. Again the states corresponding to $E_I(1.75 \text{ \AA})$ and $E_{II}(1.75 \text{ \AA})$ have two (not equally) dominant Slater determinants, whereas the states corresponding to $E_{III}(1.75 \text{ \AA})$ have weaker static correlations and just one dominant Slater determinant.

A possible reason that this problem is not evident at other bond distances is that the energy spacings between the groups of degenerate excited states are larger.

Overall the following conclusion can be made: A generic feature of the e-QEB-ADAPT-VQE is to be more “willing” to construct ansätze for less statically correlated states (where one Slater determinant is dominant). This is due to its greedy strategy to grow its ansatz with the qubit excitation evolution that decreases the energy estimate by the most at each

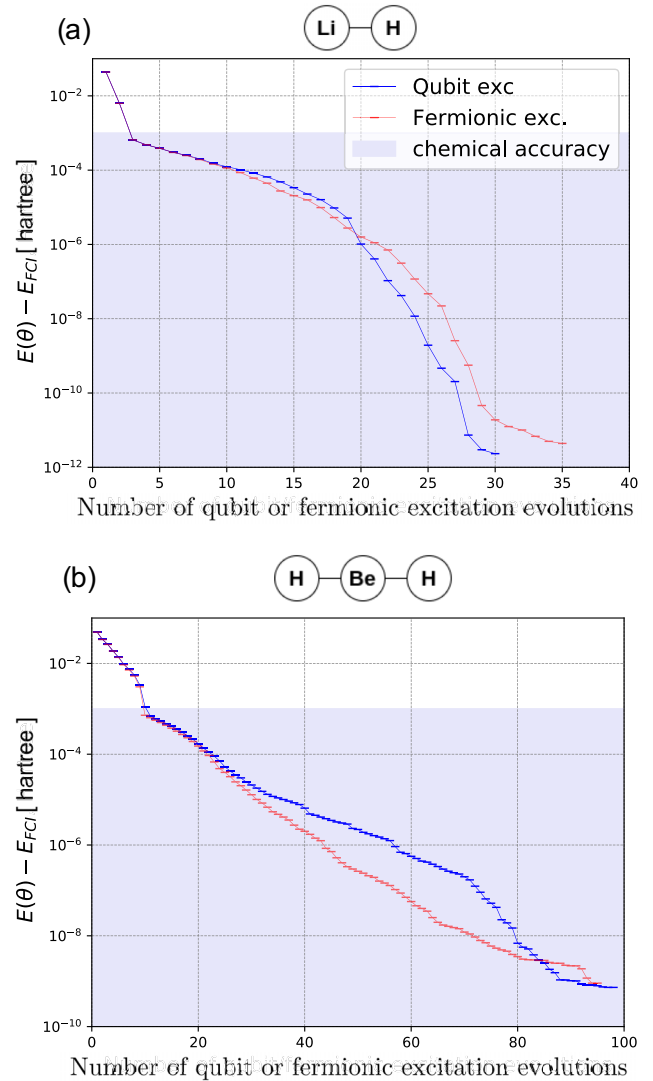


FIG. 4. Energy convergence plots for the first excited states of LiH and BeH_2 in the STO-3G basis at equilibrium bond distances of $r_{\text{Li-H}} = 1.546 \text{ \AA}$ and $r_{\text{Be-H}} = 1.316 \text{ \AA}$, respectively. The plots are obtained with the e-QEB-ADAPT-VQE for $n_{qe} = 10$.

ansatz-growing iteration. Hence, in the case when (i) the lowest energy eigenstates of an electronic Hamiltonian are ordered in two or more closely spaced (possibly degenerate) energy levels and (ii) the lowest energy level corresponds to eigenstates that have static correlations stronger than those of the eigenstates above them; the e-QEB-ADAPT-VQE might converge to one of the less statically correlated eigenstates, instead of to one with the lowest energy.

One possible solution to this problem is to add, in advance, qubit excitation evolutions that map the initial reference state to the dominant Slater determinant(s) of the target state. However, this would require *a priori* knowledge of the structure of the target state. Another possible solution is to exploit symmetries of the problem as suggested in Ref. [51].

Lastly, we note that this problem was also studied in Ref. [52].

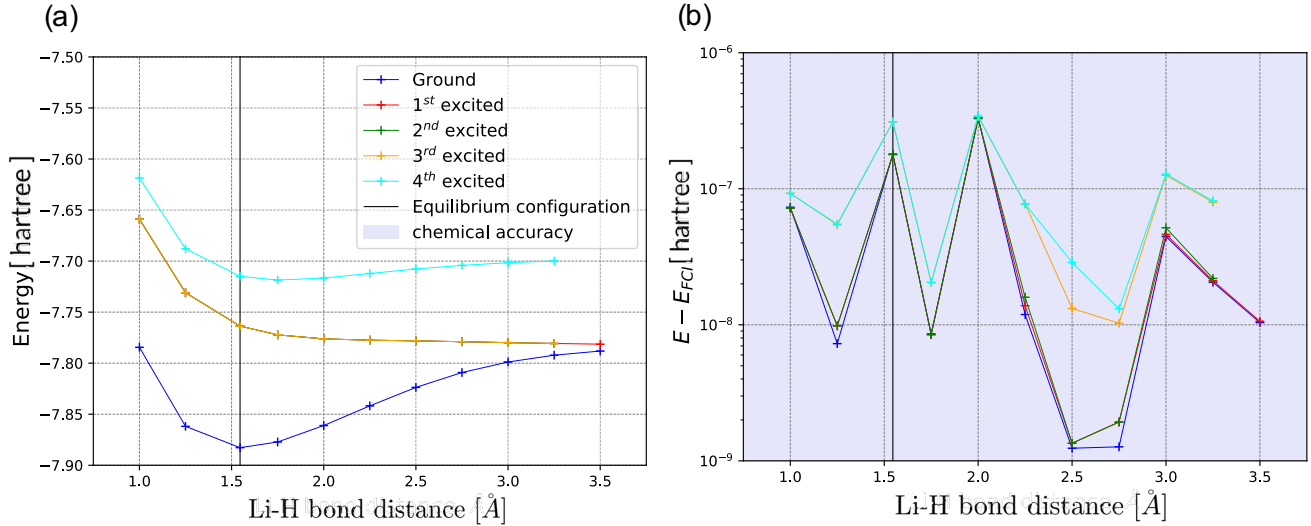


FIG. 5. (a) Energies for the five lowest energy states of LiH, in the STO-3G basis, obtained with the e-QEB-ADAPT-VQE for $\epsilon = 10^{-8}$ hartree. Note that excited states 1, 2, and 3 are degenerate. (b) Errors in the estimated energy values with respect to the FCI energies.

V. QUBIT VS FERMIONIC EXCITATION EVOLUTIONS

The use of qubit excitation evolutions by the QEB-ADAPT-VQE was motivated by the fact that they are implemented by quantum circuits that are simpler than those of fermionic excitation evolutions [25,27], and the presumption that a qubit-excitation-based ansatz can approximate an electronic wave function as well as a fermionic-excitation-based ansatz. In Ref. [25] we compared the two types of ansätze in approximating the ground states for small molecules and found that the ansätze perform similarly, in terms of accuracy. In this section, we generalize this comparison for (more strongly correlated) excited states.

Figure 4 shows energy convergence plots for the first excited states of LiH and BeH₂, at bond distances of $r_{\text{Li-H}} = 1.546 \text{ \AA}$ and $r_{\text{Be-H}} = 1.316 \text{ \AA}$, respectively. The blue (dark) plots are obtained with the e-QEB-ADAPT-VQE for $n = 10$ (the same plots as in Fig. 1), and the red (light) plots are obtained with the e-QEB-ADAPT-VQE ansatz-constructing routine, for $n = 10$, using a pool of single and double fermionic (instead of qubit) excitation evolutions. We can observe close similarity between the two types of ansätze. In the case of LiH [Fig. 4(a)] the qubit-excitation-based ansatz is slightly more accurate per number of ansatz elements, while in the case of BeH₂ [Fig. 4(b)] the fermionic-excitation-based ansatz is a bit more accurate instead. These differences are relatively small, so we derive the same conclusion as in Refs. [25,28], that qubit and fermionic excitation evolutions can approximate electronic wave functions comparably well.

VI. CONCLUSION

In this paper we proposed a modified version of the QEB-ADAPT-VQE algorithm, the e-QEB-ADAPT-VQE, designed to simulate low-lying excited molecular states.

The QEB-ADAPT-VQE relies on an initial reference state, which has a large overlap with the target ground state in order to construct an efficient ansatz. However, choosing an initial reference state that has a significant overlap with a target excited state is not as straightforward as for a target ground state. Therefore, the e-QEB-ADAPT-VQE is designed to be less dependent on the choice of an initial reference state. This is achieved by an ansatz-growing strategy that does not rely on energy-gradient evaluations, like the QEB-ADAPT-VQE, but instead on individual energy-reduction evaluations. The modified ansatz-growing strategy comes at a cost of up to a constant factor of more quantum computer measurements, as compared to the original QEB-ADAPT-VQE.

We benchmarked the performance of the e-QEB-ADAPT-VQE with classical numerical simulations, by constructing ansätze for the first excited states of LiH and BeH₂. We found that the e-QEB-ADAPT-VQE can construct highly accurate ansätze that are implemented by multiple times shallower circuits, which require multiple times fewer CNOT gates, than fixed UCC ansätze, like the UCCSD and the GUCCSD. Therefore, the e-QEB-ADAPT-VQE is especially suitable for NISQ computers, for which the number of two-qubit entangling gates, such as CNOT gates, that can be applied reliably is the current bottleneck [8].

We also found that the e-QEB-ADAPT-VQE might fail to find excited-state energies in order of increasing energy, if the excited states are ordered in closely spaced degenerate energy levels and the lower-lying excited states are more statically correlated than the states above them. This problem derives from the fact that the e-QEB-ADAPT-VQE pursues the greedy strategy to achieve a lowest estimate for the energy at each ansatz-growing iteration. Hence, the algorithm runs the risk of going along the wrong path and converging to a state which is not necessarily the one with the lowest energy. In fact, this problem will be present in any iterative-VQE protocol that relies on such a greedy strategy, including the QEB-ADAPT-VQE, the ADAPT-VQE [21], and the qubit-

ADAPT-VQE [22]. Nevertheless, this problem is unlikely to be significant, because in practice one would be interested in finding the whole spectrum of low-lying excited-state energies, so the order in which they are found is not necessarily important.

Lastly, we used the e-QEB-ADAPT-VQE ansatz-constructing routine to compare qubit-excitation-based and fermionic-excitation-based ansätze in approximating excited states. The two types of ansätze were found to perform similarly, achieving a particular accuracy with approximately the same number of qubit and fermionic excitation evolutions. These observations generalize previous results [25,28] about the equivalence of qubit and fermionic excitation evolutions in approximating electronic wave functions.

ACKNOWLEDGMENTS

The authors thank Dr. N. Mertig for useful discussions. Y.S.Y. acknowledges financial support from the EPSRC and Hitachi via CASE Studentship No. RG97399.

APPENDIX: HIGHER EXCITED STATES FOR LIH

In this section, we further benchmark the performance of the e-QEB-ADAPT-VQE by obtaining higher excited-state energies for LiH. Energy dissociation curves for the five lowest energy states of LiH in the STO-3G basis, obtained with the e-QEB-ADAPT-VQE for $n = 10$ and $\epsilon = 10^{-8}$ hartree, are plotted in Fig. 5(a). Figure 5(b) shows the corresponding errors.

The first important thing to verify in these plots is that the e-QEB-ADAPT-VQE successfully constructs accurate ansätze for all three degenerate states corresponding to the lowest excited energy level of LiH. Also, Fig. 5(b) demonstrates how the recursive error of the overlap-based method scales as more excited states are approximated. Assuming that the relative error of the e-QEB-ADAPT-VQE for each excited state is approximately the same, then the absolute error in the estimate of the energy of excited state k , E_k , should increase approximately linearly with k . Although we do not have enough excited states to check if this linear dependence is obeyed, the increase in the error is evident.

-
- [1] A. Peruzzo, J. McClean, P. Shadbolt, M.-H. Yung, X.-Q. Zhou, P. J. Love, A. Aspuru-Guzik, and J. L. O'Brien, *Nat. Commun.* **5**, 4213 (2014).
- [2] S. McArdle, S. Endo, A. Aspuru-Guzik, S. C. Benjamin, and X. Yuan, *Rev. Mod. Phys.* **92**, 015003 (2020).
- [3] J. R. McClean, J. Romero, R. Babbush, and A. Aspuru-Guzik, *New J. Phys.* **18**, 023023 (2016).
- [4] P. J. J. O'Malley, R. Babbush, I. D. Kivlichan, J. Romero, J. R. McClean, R. Barends, J. Kelly, P. Roushan, A. Tranter, N. Ding, B. Campbell, Y. Chen, Z. Chen, B. Chiaro, A. Dunsworth, A. G. Fowler, E. Jeffrey, E. Lucero, A. Megrant, J. Y. Mutus *et al.*, *Phys. Rev. X* **6**, 031007 (2016).
- [5] D. Wang, O. Higgott, and S. Brierley, *Phys. Rev. Lett.* **122**, 140504 (2019).
- [6] F. Arute, K. Arya, R. Babbush, D. Bacon, J. C. Bardin, R. Barends, S. Boixo, M. Broughton, B. B. Buckley, D. A. Buell *et al.*, *Science* **369**, 1084 (2020).
- [7] K. Bharti, A. Cervera-Lierta, T. H. Kyaw, T. Haug, S. Alperin-Lea, A. Anand, M. Degroote, H. Heimonen, J. S. Kottmann, T. Menke *et al.*, *Rev. Mod. Phys.* **94**, 015004 (2022).
- [8] J. Preskill, *Quantum* **2**, 79 (2018).
- [9] F. Arute, K. Arya, R. Babbush, D. Bacon, J. C. Bardin, R. Barends, R. Biswas, S. Boixo, F. G. Brandao, D. A. Buell *et al.*, *Nature (London)* **574**, 505 (2019).
- [10] H.-S. Zhong, H. Wang, Y.-H. Deng, M.-C. Chen, L.-C. Peng, Y.-H. Luo, J. Qin, D. Wu, X. Ding, Y. Hu *et al.*, *Science* **370**, 1460 (2020).
- [11] T. Helgaker, P. Jorgensen, and J. Olsen, *Molecular Electronic-Structure Theory* (Wiley & Sons, New York, 2014).
- [12] U. Dorner, R. Demkowicz-Dobrzanski, B. J. Smith, J. S. Lundeen, W. Wasilewski, K. Banaszek, and I. A. Walmsley, *Phys. Rev. Lett.* **102**, 040403 (2009).
- [13] A. Aspuru-Guzik, A. D. Dutoi, P. J. Love, and M. Head-Gordon, *Science* **309**, 1704 (2005).
- [14] D. S. Abrams and S. Lloyd, *Phys. Rev. Lett.* **83**, 5162 (1999).
- [15] C. Hempel, C. Maier, J. Romero, J. McClean, T. Monz, H. Shen, P. Jurcevic, B. P. Lanyon, P. Love, R. Babbush, A. Aspuru-Guzik, R. Blatt, and C. F. Roos, *Phys. Rev. X* **8**, 031022 (2018).
- [16] J. Romero, R. Babbush, J. R. McClean, C. Hempel, P. J. Love, and A. Aspuru-Guzik, *Quantum Sci. Technol.* **4**, 014008 (2018).
- [17] J. Lee, W. J. Huggins, M. Head-Gordon, and K. B. Whaley, *J. Chem. Theory Comput.* **15**, 311 (2019).
- [18] P.-L. Dallaire-Demers, J. Romero, L. Veis, S. Sim, and A. Aspuru-Guzik, *Quantum Sci. Technol.* **4**, 045005 (2019).
- [19] I. O. Sokolov, P. K. Barkoutsos, P. J. Ollitrault, D. Greenberg, J. Rice, M. Pistoia, and I. Tavernelli, *J. Chem. Phys.* **152**, 124107 (2020).
- [20] A. Anand, P. Schleich, S. Alperin-Lea, P. W. Jensen, S. Sim, M. Díaz-Tinoco, J. S. Kottmann, M. Degroote, A. F. Izmaylov, and A. Aspuru-Guzik, *Chem. Soc. Rev.* **51**, 1659 (2022).
- [21] H. R. Grimsley, S. E. Economou, E. Barnes, and N. J. Mayhall, *Nat. Commun.* **10**, 3007 (2019).
- [22] H. L. Tang, V. O. Shkolnikov, G. S. Barron, H. R. Grimsley, N. J. Mayhall, E. Barnes, and S. E. Economou, *PRX Quantum* **2**, 020310 (2021).
- [23] S. Sim, J. Romero, J. F. Gonthier, and A. A. Kunitsa, *Quantum Sci. Technol.* **6**, 025019 (2021).
- [24] D. Claudino, J. Wright, A. McCaskey, and T. S. Humble, *Front. Chem.* **8**, 606863 (2020).
- [25] Y. S. Yordanov, V. Armaos, C. H. Barnes, and D. R. Arvidsson-Shukur, *Commun. Phys.* **4**, 228 (2021).
- [26] L.-A. Wu and D. Lidar, *J. Math. Phys.* **43**, 4506 (2002).
- [27] Y. S. Yordanov, D. R. M. Arvidsson-Shukur, and C. H. W. Barnes, *Phys. Rev. A* **102**, 062612 (2020).
- [28] R. Xia and S. Kais, *Quantum Sci. Technol.* **6**, 015001 (2020).
- [29] F. Zhang, N. Gomes, Y. Yao, P. P. Orth, and T. Iadecola, *Phys. Rev. B* **104**, 075159 (2021).
- [30] H. H. S. Chan, N. Fitzpatrick, J. Segarra-Martí, M. J. Bearpark, and D. P. Tew, *Phys. Chem. Chem. Phys.* **23**, 26438 (2021).

- [31] K. M. Nakanishi, K. Mitarai, and K. Fujii, *Phys. Rev. Res.* **1**, 033062 (2019).
- [32] P. J. Ollitrault, A. Kandala, C.-F. Chen, P. K. Barkoutsos, A. Mezzacapo, M. Pistoia, S. Sheldon, S. Woerner, J. M. Gambetta, and I. Tavernelli, *Phys. Rev. Res.* **2**, 043140 (2020).
- [33] S. Liu, S.-X. Zhang, C.-Y. Hsieh, S. Zhang, and H. Yao, [arXiv:2111.13719](https://arxiv.org/abs/2111.13719).
- [34] R. M. Parrish, E. G. Hohenstein, P. L. McMahon, and T. J. Martínez, *Phys. Rev. Lett.* **122**, 230401 (2019).
- [35] P. Jordan and E. Wigner, *Z. Phys.* **47**, 631 (1928).
- [36] S. B. Bravyi and A. Y. Kitaev, *Ann. Phys.* **298**, 210 (2002).
- [37] J. T. Seeley, M. J. Richard, and P. J. Love, *J. Chem. Phys.* **137**, 224109 (2012).
- [38] B. Klahn and W. A. Bingel, *Theor. Chim. Acta* **44**, 9 (1977).
- [39] J. R. McClean, Z. Jiang, N. C. Rubin, R. Babbush, and H. Neven, *Nat. Commun.* **11**, 636 (2020).
- [40] J. R. McClean, M. E. Kimchi-Schwartz, J. Carter, and W. A. de Jong, *Phys. Rev. A* **95**, 042308 (2017).
- [41] J. I. Colless, V. V. Ramasesh, D. Dahlen, M. S. Blok, M. E. Kimchi-Schwartz, J. R. McClean, J. Carter, W. A. de Jong, and I. Siddiqi, *Phys. Rev. X* **8**, 011021 (2018).
- [42] O. Higgott, D. Wang, and S. Brierley, *Quantum* **3**, 156 (2019).
- [43] T. Jones, S. Endo, S. McArdle, X. Yuan, and S. C. Benjamin, *Phys. Rev. A* **99**, 062304 (2019).
- [44] L. Cincio, Y. Subaşı, A. T. Sornborger, and P. J. Coles, *New J. Phys.* **20**, 113022 (2018).
- [45] C. Kokail, C. Maier, R. van Bijnen, T. Brydges, M. K. Joshi, P. Jurcevic, C. A. Muschik, P. Silvi, R. Blatt, C. F. Roos *et al.*, *Nature (London)* **569**, 355 (2019).
- [46] J. A. Nelder and R. Mead, *Comput. J.* **7**, 308 (1965).
- [47] A. Kandala, A. Mezzacapo, K. Temme, M. Takita, M. Brink, J. M. Chow, and J. M. Gambetta, *Nature (London)* **549**, 242 (2017).
- [48] R. Ditchfield, W. J. Hehre, and J. A. Pople, *J. Chem. Phys.* **54**, 724 (1971).
- [49] R. Fletcher, *Practical Methods of Optimization* (Wiley & Sons, New York, 2013).
- [50] T. Helgaker, S. Coriani, P. Jorgensen, K. Kristensen, J. Olsen, and K. Ruud, *Chem. Rev.* **112**, 543 (2012).
- [51] V. Shkolnikov, N. J. Mayhall, S. E. Economou, and E. Barnes, [arXiv:2109.05340](https://arxiv.org/abs/2109.05340).
- [52] I. G. Ryabinkin, S. N. Genin, and A. F. Izmaylov, *J. Chem. Theory Comput.* **15**, 249 (2019).